ACS Partner Journal

PHOTON SCIENCE

Editors' Choice

Open Access

This article is licensed under CC-BY-NC-ND 4.0

pubs.acs.org/photonsci

Article

A Flat Analyzer Polycapillary Spectrometer for X-ray Absorption Spectroscopy of Dilute Transition Metals at X-ray-Free Electron Lasers

Angel T. Garcia-Esparza,[▽] Jinkyu Lim,[▽] Alexander Britz, Marco Reinhard, Ryan D. Ribson, Jeffrey T. Babicz, Jr., Cali Antolini, Leland B. Gee, Quinn Claussen, Nina A. Boiadjieva, Leslie Hsiao, Jim Defever, Patrick Oppermann, Vincent Esposito, Hasan Yavas, Dean Skoien, Matthieu Chollet, Tim B. van Driel, Sanghoon Song, Diling Zhu, Dimosthenis Sokaras,* and Roberto Alonso-Mori*

Cite This: *Photon Sci.* 2026, 1, 121−129

Read Online

ACCESS | Metrics & More | Article Recommendations

ABSTRACT: X-ray absorption spectroscopy (XAS) coupled with highly intense pulses from an X-ray-free electron laser (XFEL) can be used to track ultrafast chemical dynamics. Nonetheless, measurements for dilute samples (≤1 mM) have been exceptionally challenging, as scattering background signals dominate over the sample's X-ray fluorescence. We show that femtosecond time-resolved XAS measurements of sub-millimolar transition metal solutions are now possible at the Linac Coherent Light Source (LCLS) using a high-throughput polycapillary XAS spectrometer, designed, developed, and commissioned at LCLS and the Stanford Synchrotron Radiation Lightsource (SSRL). The instrument integrates three polycapillary optics that collect and collimate X-ray fluorescence emitted from the interaction point with a high solid angle. X-ray collimated fluorescence is then selectively diffracted by coupled graphite analyzer crystals. As a result, the contribution of scattered photons is suppressed. Experiments at the Pt L_3-edge on 0.1 mM aqueous K_2PtCl_6 (delivered via a 100 μm liquid jet) were successfully performed in the laser pump X-ray probe configuration at the LCLS XCS and XPP instruments. We report the transient spectra of hexachloroplatinate within the first 10 ps after a 266 nm photoexcitation. We observed a short-lived reduced intermediate (≈2 ps). The polycapillary X-ray spectrometer at LCLS now enables the efficient study of the dynamics of ultradilute transition metals in solution. This capability opens the door to investigating plasmonic systems, photocatalysts, enzymes, and other scarce and dilute samples.

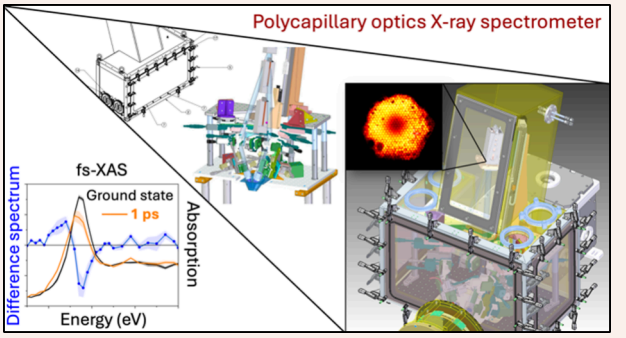

KEYWORDS: *polycapillary optics, time-resolved, X-ray absorption spectroscopy, X-ray free electron laser, ultrafast spectroscopy, LCLS, SSRL*

Downloaded via ACS Test Institution on March 27, 2026 at 14:53:33 (UTC).
See https://pubs.acs.org/sharingguidelines for options on how to legitimately share published articles.

INTRODUCTION

X-ray absorption spectroscopy (XAS) is a powerful technique for probing electronic and geometric structural properties of molecules and matter with elemental specificity.[1,2] It provides detailed insights into oxidation states, chemical bonding, symmetry, and coordination environment, making it broadly applicable across various fields, including materials science, chemistry, physics, and biology.[1,3,4] The deep penetration of hard X-rays (>5 keV) enables the study of bulk properties under realistic conditions, including high pressure and temperature environments, enabling so-called in situ and operando experiments. A key advantage of the technique is its applicability to a wide range of sample types and in various forms and states, as well as its compatibility with diverse sample environments. These characteristics make XAS an invaluable tool for investigating complex functional systems under conditions that mimic their real-world operating environments.[5,6]

The development of X-ray free-electron lasers (XFELs) has significantly advanced time-resolved X-ray measurements by providing ultrafast temporal resolution and enhanced brilliance, exceeding synchrotron sources by orders of magnitude.[4,7,8] Facilities like the Linac Coherent Light Source (LCLS) generate femtosecond-long intense and coherent X-ray pulses that enable time-resolved measurements to study

Received: September 4, 2025
Revised: November 15, 2025
Accepted: November 18, 2025
Published: December 14, 2025

ACS Publications

© 2025 The Authors. Co-published by ShanghaiTech University and American Chemical Society

https://doi.org/10.1021/photonsci.5c00024
Photon Sci. 2026, 1, 121−129

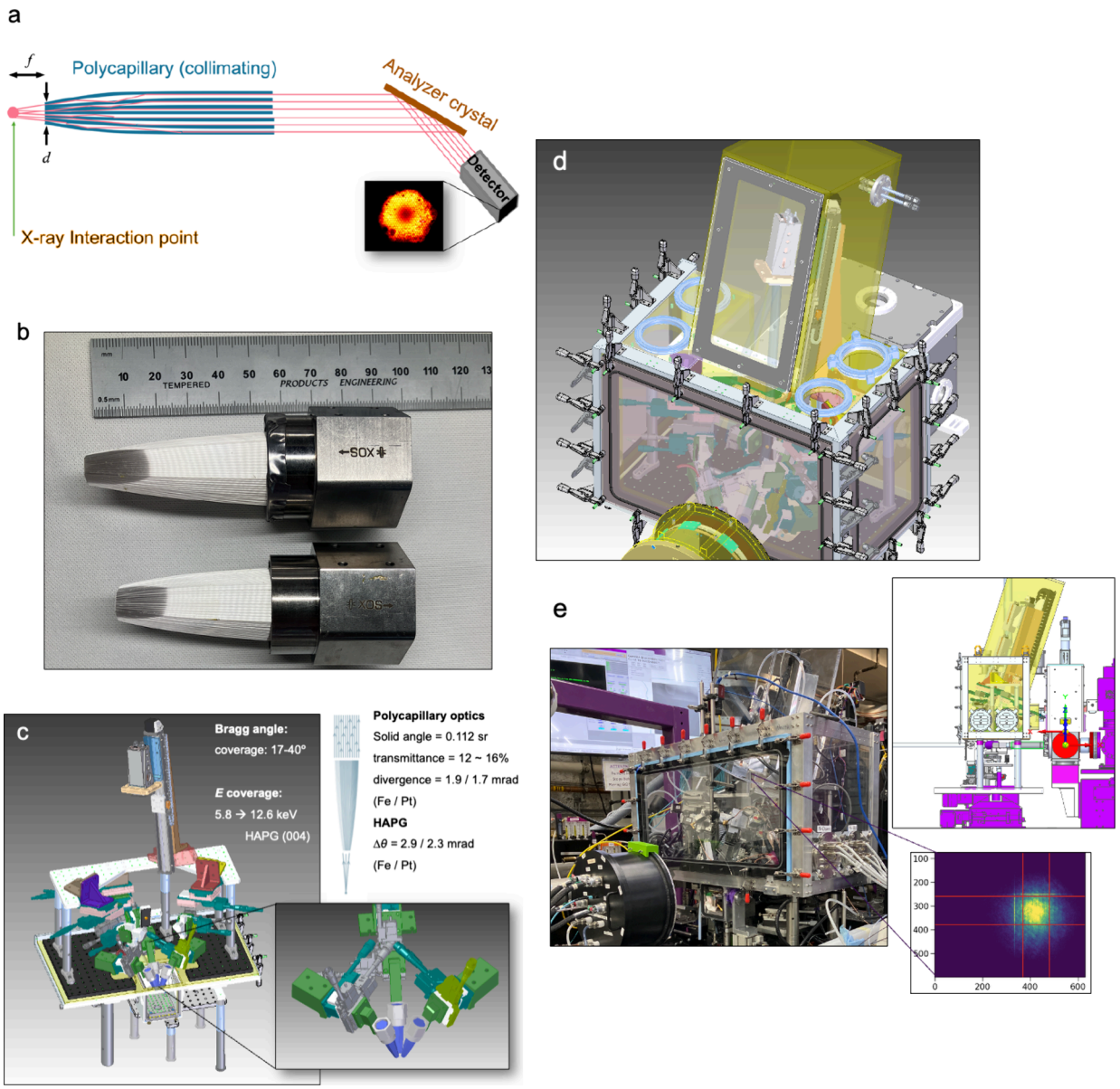

Figure 1. (a) Schematic of the concept of polycapillary optics with crystal analyzers. (b) Polycapillary optics and (c–e) technical drawings and model of the polycapillary X-ray spectrometer (PCXS) for studies of dilute transition metals. (b–d) Three polycapillary optics, three crystal analyzers (highly oriented or highly annealed pyrolytic graphite), and one ePix100 detector are installed in the (d) He enclosure. Components are automated with over 20 motors for alignment and signal optimization. (e) The instrument sits above the liquid jet instrument in the standard configuration used at the XPP and XCS instruments at LCLS. A picture of the spectrometer installed at the XCS instrument at LCLS is shown with a heat map as an example of the collected signal obtained after alignment and signal optimization.

fundamental physical and chemical phenomena such as bond breaking/formation, charge transfer, and phase transitions.[3,4,7,9] Using the femtosecond pulses from an XFEL, time-resolved XAS enables the direct observation of charge dynamics in, for example, biological systems, with the potential to reveal previously unobservable intermediate states in energy conversion systems.[10−16]

Ultrafast time-resolved hard X-ray XAS experiments at LCLS are routinely carried out at the X-ray correlation spectroscopy (XCS) instrument.[17−19] For solution-phase chemistry studies, the liquid jet endstation (LJE),[19] a standardized experimental configuration, has been extensively adopted in user experiments to maximize throughput, ensure efficient use of highly competitive LCLS beamtime, and improve the overall success rate of time-resolved measurements.[12,19−21] These time-resolved experiments are typically conducted using the pump-probe methodology, in which an optical laser pulse initiates a photochemical reaction (pump) and temporally delayed X-ray pulses probe the subsequent response of the system.[17,18,22] The incident X-ray energy is scanned across the absorption edge of interest and the X-ray absorption is typically measured in total fluorescence yield (TFY) mode using a pixelated 2D detector.[8,17,18] Specifically, an ePix100 2D detector recorded all emitted and scattered photons from the sample. Because this detector provides limited energy resolution, it cannot distinguish between the X-ray fluorescence of interest and the scattered photons from the incoming beam.[20] This standard TFY configuration is highly efficient due to its large solid angle (~0.4 sr) and has been widely used at the LCLS, particularly for solution-phase samples with

https://doi.org/10.1021/photonsci.5c00024
Photon Sci. 2026, 1, 121−129

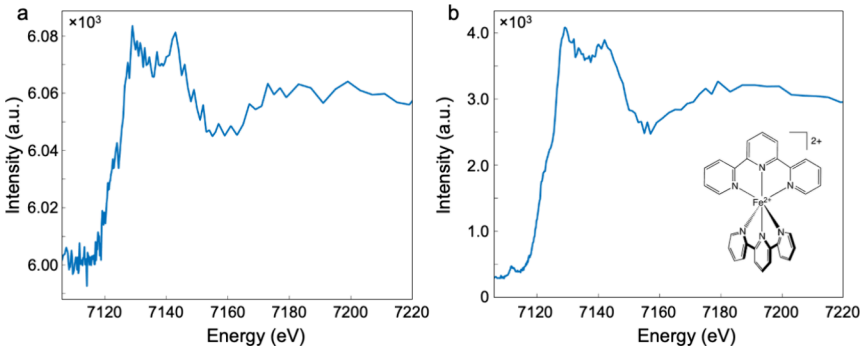

Figure 2. Results of a polycapillary-based spectrometer prototype at SSRL beamline 15-2. (a) Steady-state Fe K-edge XAS obtained in total fluorescence yield (TFY) detection mode with a photodiode from a 0.1 mM $[Fe(terpy)_2]^{2+}$ complex (2,2′:6′,2″-terpyridine) delivered via 100 μm liquid jet configuration. (b) The partial fluorescence yield (PFY) recorded using one polycapillary (PC) optic and one highly oriented pyrolytic graphite crystal analyzer (HOPG) with a PILATUS 300k detector (single scan with 1 s acquisition per energy point, 10^{13} photons per second).

concentrations in the several millimolar range. However, for highly dilute samples (≪1 mM) the TFY mode faces significant limitations.[3] In such cases, the X-ray fluorescence signal is often overwhelmed by dominant scattering contributions from the sample's environment (such as the solvent). This background signal can drastically reduce the signal-to-noise ratio, compromising both the data quality and experimental efficiency. These challenges are particularly pronounced in time-resolved experiments, where transient spectra typically show small spectral differences, while limited sample volumes further constrain experimental conditions.[3]

The partial fluorescence yield (PFY) XAS[23] mode selectively detects photons corresponding to a specific emission line, effectively suppressing background signals such as scattering and X-ray fluorescence from other elements.[23] Recently, members of our team demonstrated the successful implementation of PFY XAS at an XFEL using a short radius Johann geometry.[24] Another implementation at LCLS is a von Hamos spectrometer with multiple cylindrically bent analyzer crystals that provide wavelength-dispersive detection on a 2D position-sensitive detector suited for X-ray emission spectroscopy (ePix100).[22,25] Nonetheless, the low solid angle per eV restricts the X-ray fluorescence collected, making it suboptimal for time-resolved XAS.[3] Moreover, attempts to increase the collection efficiency through multiple analyzer crystals are limited by geometric constraints and the increased complexity of the spectrometers.

To overcome the limitations associated with detecting very diluted samples in time-resolved XAS, herein we report the design, development, and implementation of a hard X-ray spectrometer based on polycapillary optics (PCO), optimized for experiments at LCLS with sample concentrations far below the 1 mM range. The high-throughput spectrometer, referred to as the PCO X-ray spectrometer (PCXS), employs three large acceptance angle PCO to collect and collimate fluorescence X-ray photons emitted from the X-ray interaction point with a high solid angle coverage. The collimated X-rays are directed onto flat graphite Bragg crystals (either highly oriented, HOPG, or highly annealed, HAPG, pyrolytic graphite), chosen for their high integral reflectivity. As a result, X-ray fluorescence photons are selectively diffracted toward a detector, effectively achieving background suppression by filtering out scattered radiation and providing an optimal balance between energy selectivity and photon throughput. Consequently, the PCXS achieves orders of magnitude improvement in signal-to-background ratio compared to the standard TFY configuration.[26−31]

To benchmark performance and demonstrate the unique class of experiments that are now possible at LCLS, we conducted time-resolved experiments on an aqueous solution of potassium hexachloroplatinate (K_2PtCl_6, 0.1 mM) delivered to the interaction point via a 100 μm liquid jet. The system was photoexcited at 266 nm, and picosecond-resolved transient Pt L_3-edge spectra were collected. Kinetic traces measured at 11568.0 eV reveal a biexponential decay, resolving a short-lived reduced intermediate with a ∼2 ps lifetime and a long-lived excited state persisting beyond 10 ps. These results demonstrate that the PCXS dramatically enhances the quality of ultrafast XAS measurements on dilute systems, expanding the reach of time-resolved studies at LCLS to a broader class of samples.

RESULTS AND DISCUSSION

The schematic in Figure 1 shows the concept of selectively collecting and collimating the divergently emitted X-ray fluorescence from the sample/X-ray interaction point (IP) using PCO; then, the collimated X-rays are analyzed with a Bragg crystal optic. In our concept, the targeted X-ray photons are directed onto energy-selective highly oriented (HOPG) or highly annealed pyrolytic graphite (HAPG) crystals with high integral reflectivity. The effective suppression of background scattering results from the diffraction of specific energy lines at the HOPG/HAPG analyzers and is due to the geometrically restricted acceptance angle of the collimating PCO.

A first prototype consisting of a single polycapillary optic with one single HOPG analyzer was developed and commissioned at SSRL beamline 15-2 as a proof-of-concept.[2,32] First, Figure 2b shows the Fe K-edge X-ray absorption near edge structure (XANES) spectrum collected in the TFY mode using a PIPS diode from a single energy scan (1 s per point) of a 0.1 mM aqueous solution of a $[Fe(terpy)_2]^{2+}$ complex delivered at the X-ray IP via a 100 μm round liquid jet. Second, Figure 2c shows the same sample's PFY measured under the same acquisition conditions using the prototype polycapillary X-ray spectrometer with a PILATUS 2D detector. The PCXS resolves the pre-edge feature below 7120.0 eV and the rising edge shoulder near 7125.0 eV.[20,33−35] Overall, the visual inspection of the spectral quality shows substantial noise reduction and demonstrates that the signal-to-background

https://doi.org/10.1021/photonsci.5c00024
Photon Sci. 2026, 1, 121−129

ratio improved from 0.01 to 15 (S/B = $(I_S - I_B)/I_B$; I_S = edge-jump magnitude, I_B = intensity below pre-edge).

Tables 1−3 summarize the measured properties of the PCO and the analyzer crystals that were characterized at SSRL

Table 1. Focal Spot and Depth of the Polycapillary Optics Measured at the Fe K-Edge and Pt L_3-Edge using $K_3Fe(CN)_6$ and K_2PtCl_4 Standard Samples in Aqueous Solution

	Focal spot (μm)	Focal depth (μm)
Fe K-edge		
PCO-long	146	1708
PCO-short	168	2075
Pt L_3-edge		
PCO-long	99	1244
PCO-short	113	1700

beamline 15-2 at the Fe K-edge and Pt L_3-edge using 0.1−20 mM $K_3Fe(CN)_6$ and 0.1−20 mM K_2PtCl_4 in water (neutral pH), respectively. Two types of X-ray optics were procured from XOS (Figure 1b): a "short" PCO, and a "long" PCO. The long PCO is 90 mm long, and the short one is 10 mm shorter. The PCO tip-sizes are 4 mm hexagons with a focal length that varies from 18 to 21 mm depending on the optics size. The solid angle of an n-gonal pyramid ($\Omega = 2\pi - 2n \arctan[\tan(\pi/n)/(1+(r^2/h^2))^{1/2}]$) with a pyramid height h can be obtained, where the base of the pyramid is an n-sided polygon of r circumradius. The extracted solid angle of coverage of each PCO is 0.112 sr, corresponding to a coverage of approximately 0.9%. Table 1 reports the measured focal spot and depth of the two types of PCOs recorded at the Fe K-edge (7112 eV) and the Pt L_3-edge (11564 eV). The focal depth is how much motion is required across the polycapillary axis direction to lose ca. 50% of the intensity. The focal spot of the short PCO is on average 17% and 22% larger than the long one at the Fe K-edge and the Pt L_3-edge, respectively.

The divergence ($E/\Delta E = \tan\theta/\Delta\theta$) of the short PCO is on average approximately two-fold larger than the long one for the studied energy ranges (Table 2). The divergence of the PCOs

Table 2. Divergence of the Polycapillary Optics at the Fe K-Edge and Pt L_3-Edge Using $K_3Fe(CN)_6$ and K_2PtCl_4 Standard Samples in Aqueous Solution[a]

	ΔE (eV)	$E/\Delta E$	$\Delta\theta$ (mrad)
Fe K-edge			
PCO-long	6.2	1033	1.9
PCO-short	16.0	400	4.9
Pt L_3-edge			
PCO-long	21.6	437	1.7
PCO-short	41.3	229	3.3

[a]The elastic energy scan was performed using a Ge(333) crystal with an energy resolution of 0.15 eV, Bragg angle of 62.77° at 6403.84 eV for Fe. The energy resolution is 0.22 eV, Bragg angle of 37.09° at 9442.3 eV for Pt.

was extracted by pairing them with a Ge(333) analyzer: because the analyzer's energy broadening is only ∼0.15 eV, the measured resolution directly reflects the beam divergence. When the step size of XAS (edge jump) is compared using a 20 mM $K_3Fe(CN)_6$ sample and a diode detector, the extracted transmittance of the long and short PCO for the Fe−Kα_1 is ≈16% when considering the absorption by air. Overall, the PCO transmission remains reasonable for experiments using incident X-rays with an energy range of ca. 6−12 keV. Table 3

Table 3. Energy Resolution of Graphite HAPG and HOPG Crystal Analyzers at the Fe K-Edge and Pt L_3-Edge Using $K_3Fe(CN)_6$ and K_2PtCl_4 Standard Samples in Aqueous Solution

			ΔE (eV)	$E/\Delta E$	$\Delta\theta$ (mrad)
Fe K-edge					
Graphite (004)[a]	PCO-long	HAPG	26	248	2.9
		HOPG	133	48	14.7
	PCO-short	HAPG	51	127	5.6
		HOPG	157	41	17.3
Graphite (002)[b]	PCO-long	HAPG	154	42	7.2
		HOPG	320	20	15.1
	PCO-short	HAPG	198	32	9.3
		HOPG	390	16	18.4
Pt L_3-edge					
Graphite (004)[c]	PCO-long	HAPG	51	186	2.3
		HOPG	390	24	17.6
	PCO-short	HAPG	114	83	5.1
		HOPG	420	22	18.9

[a]35.26° at 6403.84 eV. [b]16.78° at 6403.84 eV. [c]23.05° at 9442.3 eV.

shows the energy resolution of the energy-selective graphite crystals with a high integral reflectivity. The energy resolution was benchmarked using graphite(004) and graphite(002) with the short and long PCOs for Fe Kα and Pt Lα of the $K_3Fe(CN)_6$ and K_2PtCl_4 aqueous samples. Overall, the HAPG shows better energy resolution than the HOPG crystal analyzers with a smaller $\Delta\theta$. Based on the promising results obtained at the synchrotron, we therefore proceeded with the design, development, and commissioning of a new PCXS for the XPP and XCS instruments at LCLS.

Figure 1c and e shows the technical drawings and model for the PCXS instrument. The instrument is designed for a Bragg angle coverage of 17−40°, corresponding to an energy range of 5.8−12.6 keV when using HAPG graphite(004). As previously discussed, the PCO performance exhibited a solid angle coverage of 0.112 sr, a transmittance of ≈16%, and a divergence of 1.9/1.7 mrad (Fe/Pt), and the HAPG analyzer has a mosaicity of 2.9/2.3 mrad (Figure 1c). One of the advantages of this system is that we can collect efficiently large energy ranges (e.g., extended X-ray absorption fine structure, EXAFS) and change from edge to edge without re-aligning. The main components are three motorized PCO, three motorized graphite crystal analyzers, three motorized positioning photodiode detectors, and one motorized ePix100 detector. All the main components of the instrument are housed in an airtight He enclosure, and all parts are mounted on an optical table using optical posts/holders (Figure 1d). The PLC controller for the +20 motors is mounted outside of the He box, and all the power and control connections are connected using feedthroughs. The PLC is remotely controlled and programmed via ethernet using Python commands and a

https://doi.org/10.1021/photonsci.5c00024
Photon Sci. 2026, 1, 121−129

custom-made graphical user interface. The PCXS was designed to sit on top of the liquid jet delivery instrument developed for the standard configurations used at the XCS and XPP hutches at LCLS (Figure 1e).[19] The design permits an X-ray forward scattering detector to be placed near the IP with a few millimeters' tolerance to the front of a removable panel for access to the components inside the He box. Alignment testing of the PCO with a 20 mM $K_3Fe(CN)_6$ aqueous liquid jet (150 μm) demonstrated the successful acquisition of the Fe Kα in the two-dimensional detector (Figure 1e, inset).

Figure 3 shows the UV-Vis spectra characterization of the aqueous potassium hexachloroplatinate ($Pt^{IV}Cl_6^{2-}$) sample

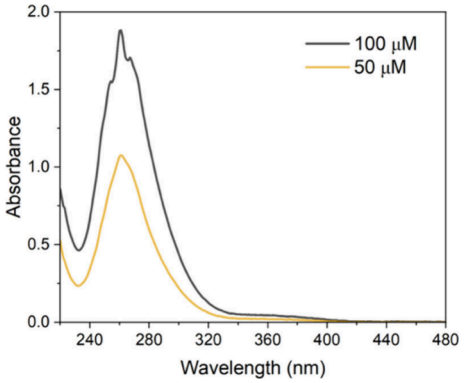

Figure 3. UV-Vis spectroscopy of aqueous K_2PtCl_6 in water.

selected as a reference standard benchmark. The spectrum is consistent with those in the literature and contains overlapping ligand-to-metal charge transfer (LMCT) bands and d-d transitions.[36−41] Based on the literature, the absorption rapidly increases below 220 nm and it is attributed to a transition from ligand π-orbitals to vacant π*-orbitals mainly localized on the central atom.[39] The most intense band at 261 nm is ascribed to transitions from the ligand π-orbitals to the e_g*-orbitals of the central ion. The broad and less intense shoulder above 350 nm has been assigned to d-d transitions.[36]

Figure 4 shows the first test at LCLS using a second prototype consisting of a single PCO and a single HOPG crystal analyzer at the XPP instrument, using $Pt^{IV}Cl_6^{2-}$ in water delivered via a 100 μm liquid jet. A direct comparison with the standard configuration using an ePix100 detector was performed to compare and benchmark the performance of the instrument to resolve diluted signals at the XFEL. The fluorescence is measured in TFY mode in the standard LCLS configuration with the ePix100 integrating all incoming signals without distinguishing X-ray photon energies.[20] Hence, the recorded fluorescence is completely dominated by the background scattering from the environment (Figure 4a). It becomes clear that, when using the PCO+HOPG system, measuring photons corresponding to specific emission of the absorbing element effectively suppresses background signals from scattering and X-ray fluorescence from other elements (Figure 4b), as observed in the background intensity level decreasing by approximately two orders of magnitude before the main edge. The PCO-collimated X-rays are directed onto the energy-selective graphite crystal (e.g., HOPG) providing a reasonable balance between energy selectivity and photon throughput; thus, filtering out scattered radiation and effectively achieving background suppression. The elastic and Compton scattering suppression is achieved through the

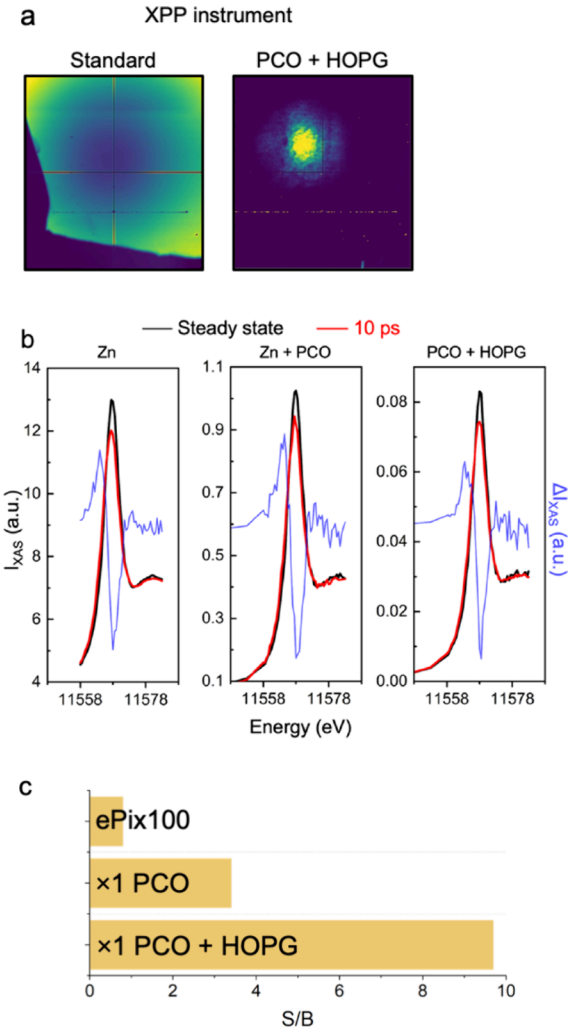

Figure 4. Polycapillary X-ray spectrometer prototype at the XPP instrument (LCLS) with one polycapillary optic (PCO) and one HOPG crystal analyzer. (a) The ePix100 detector heat map obtained in TFY detection mode from a 1 mM K_2PtCl_6 standard sample delivered via a 100 μm liquid jet; an example of the signal obtained from a single PCO plus one HOPG crystal analyzer is shown for reference. (b) Steady-state and the transient Pt L_3-edge XAS at 10 ps after 266 nm laser pump photoexcitation in TFY using a Zn filter with the ePix100 detector, in PFY using a Zinc filter with one PCO, and using one PCO plus HOPG crystal analyzer (average of 2 scans, 262 s per scan, 524 s total acquisition time). The difference spectra obtained from the subtraction of the "on" spectrum from the "off" spectrum is presented to highlight (c) the improvements of the signal-to-background ratio in the measurements when using the polycapillary spectrometer.

selective diffraction of fluorescence lines at the graphite crystals and geometrically due to the restricted acceptance angle of the collimating PCO. We recorded in such a PFY mode the 10 ps transient XANES of 1 mM K_2PtCl_6 in an aqueous 100 μm liquid jet with and without the PCO+HOPG after 266 nm laser-pump photoexcitation (Figure 4b). As a result, when using PCO+HOPG, the background diminishes to a value close to zero. A one-order-of-magnitude improvement in the signal-to-background ratio was obtained when compared to the prototypical standard configuration operating with the TFY detection mode (Figure 4c).[12,19−21,26−31]

https://doi.org/10.1021/photonsci.5c00024
Photon Sci. 2026, 1, 121−129

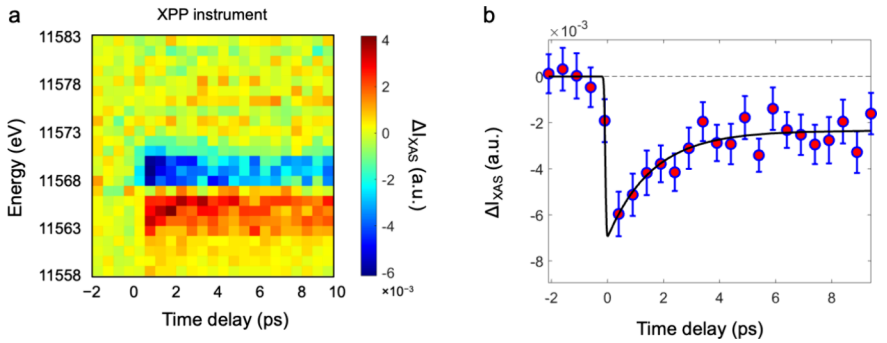

Figure 5. Ultrafast time-resolved Pt L_3-edge XAS at the XPP instrument. (a) Femtosecond time-resolved XAS kinetic map and (b) the time delay trace at 11568.0 eV obtained from 1 mM K_2PtCl_6 in a 100 μm liquid jet (biexponential fit, R^2 = 0.9999, τ_1 = 2 ± 1 ps). The error bars were extracted from the standard error of the normalized and averaged off- and on-spectra at each time delay, separately. Then, the error was propagated for the average "off" state. Finally, the errors of the "on" spectra and the "off" spectrum were used to get the error on the difference spectra (the full dataset is the result of 10 scans, 506 s acquisition time per scan, one POC, and one HOPG crystal).

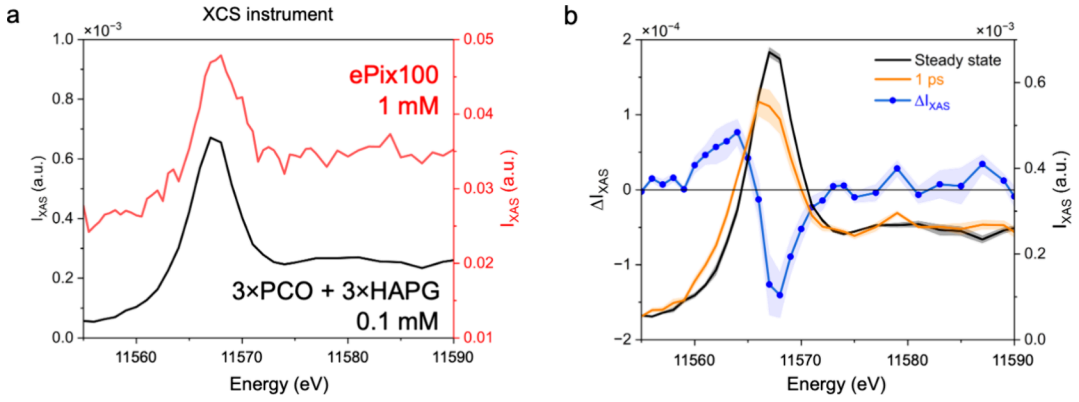

Figure 6. (a) Steady-state Pt L_3-edge XAS of 1 mM (average of 5 scans, 400 s per scan, 2000 s total acquisition time, 100 energy points) and 0.1 mM K_2PtCl_6 (average of 2 scans, 534 s per scan, 1068 s total acquisition time, 89 energy points) with and without the use of three PCOs and three HAPG crystal analyzers at the XCS instrument with the optimized PCXS. (b) Steady-state ("off") and transient Pt L_3-edge XAS at 1 ps ("on") after 266 nm laser pump photoexcitation of aqueous 0.1 mM K_2PtCl_6 in a 100 μm liquid jet. The difference spectrum is obtained from the subtraction of the "on" state at 1 ps from the "off" steady-state condition. The standard error is shown as a shaded area for all signals (average of 2 scans, 534 s acquisition time per scan).

Figure 5 shows the fs time-resolved XAS charge dynamics and kinetics of a K_2PtCl_6 sample in water recorded using the XPP instrument. After 266 nm UV-light photoexcitation, there are clear spectral differences below 10 ps, as observed in the two-dimensional kinetic heat map (Figure 5a). The presented data are the result of 10 scans of 506 s acquisition time per scan, i.e., a full dataset of reasonable quality obtained in one and a half hours of beamtime using a single PCO and a single HOPG analyzer prototype. The 2D difference map is the unscaled difference "on" minus "off" with the average difference at negative time delays subtracted (< −0.5 ps). The kinetic trace in Figure 5b is the unscaled average of the resulting difference map around the indicated energy range. All data were normalized to the scattering water ring. The biexponential decay function used to fit the kinetics trace at 11568.0 eV resolves a fast component τ_1 = 2 ± 1 ps, while we are unable to extract a slower time constant due to the limited time range of <10 ps (Figure 5b). A second time constant was nonetheless required to account for the observed persisting difference signal, and a sufficiently large value was arbitrarily fixed at τ_2 = 10 ns.

Figure 6 shows the steady-state and time-resolved Pt L_3-edge XANES of 1 and 0.1 mM K_2PtCl_6 aqueous solution delivered via a 100 μm liquid jet at the XCS instrument at LCLS using the optimized PCXS system. Figure 6a compares the steady-state Pt L_3-edge spectrum of 1 mM K_2PtCl_6 obtained in the standard configuration vs. the spectrum of 0.1 mM K_2PtCl_6 acquired using the PCXS with three PCO plus three HAPG with the ePix100 detector. From a qualitative visual inspection, the PCXS instrument enhances the signal of the ten-fold diluted sample resolving the spectrum of a sample with sub-mM concentration. The PCXS signal is the result of the average of two energy scans with a 534 s acquisition time per scan. In other words, less than 20 min of collection were required to record and resolve the transient *fs*-resolved Pt L_3-edge XANES of 0.1 mM K_2PtCl_6 at 1 ps after 266 nm laser photoexcitation. The difference spectrum in Figure 6b is directly the unscaled difference between the laser "on" and laser "off". By normalization to the edge jump, the maximum difference signal at 11568.0 eV is ≈40% of the edge jump. We performed power titrations to confirm the linear response of the system under the selected laser fluence. The Pt L_3-edge results from a $2p_{3/2}$ electron promotion to the 5d orbital, i.e., the so-called "white-line". The white line intensity correlates to the occupancy of Pt 5d orbitals; hence, it provides direct information on the oxidation state and the local environment of the metal.

https://doi.org/10.1021/photonsci.5c00024
Photon Sci. 2026, 1, 121−129

Using ultrafast transient absorption spectroscopy (TAS), laser flash photolysis, and photoelectron spectroscopy,[36−41] the proposed key aqueous photochemical reaction of $Pt^{IV}Cl_6^{2-}$ in the literature is an inner-sphere electron transfer and subsequent photoaquation.[36,39] Hexachloroplatinate is a $5d^6$ low-spin octahedral complex. It was first suggested that the homolysis of a Pt−Cl bond is the primary photoreaction in water, acetonitrile, and chloroform solvents. Later, it was established that photoaquation is the most likely overall photochemical process, eventually resulting in the generation of $Pt^{IV}Cl_5(H_2O)^-$ complex with $Pt^{III}Cl_{4-n}X_n$ (n = 1-3; X=OH^-, H_2O) as the most probable chain carrier as a function of the experimental conditions (e.g., irradiation wavelength, power density, and pH).[36] Ultrafast TAS studies of aqueous hexachloroplatinate using 355 nm resulted in two absorption bands at 440 and 640 nm, ascribed to an intermediate showing a lifetime of 210 ps. Femtosecond TAS with 405 nm photoexcitation showed broad transient absorption bands (445, 500, 550, 650, and 760 nm) that decayed completely in 800 ps. From their kinetic traces, three lifetimes of 600 fs, 8.6 ps, and 220 ps were extracted from a global fit. A total of four intermediates have been invoked to describe the TAS experiments, where the latter two species evolve in the microsecond time domain.[36,38,39]

The formation of a $Pt^{III}Cl_5^{2-}(D_{3h})$ complex was first proposed as the starting point for the photoaquation. The reported primary reactions of aqueous hexachloroplatinate after laser excitation at 405 nm are the fast formation of an Adamson's primary radical pair with the structure $[Pt^{III}Cl_5^{2-}(C_{4\,V})\cdots Cl^{\bullet}]$ from the Franck-Condon state, i.e., hot $[Pt^{IV}Cl_6^{2-}]^*(^3T_{1g})$ state. Based on photolysis experiments in methanol and ethanol, the formation of the $Pt^{III}Cl_5^{2-}(C_{4\,V})$ complex was ruled out, and the radical pair generation was found consistent with quantum chemical calculations of plausible Pt(III) intermediates. Fundamentally, the precise nature of the transient intermediate is still debatable, and the photolysis mechanism is not firmly established.[36]

Here, our femtosecond time-resolved XAS (fs-TR-XAS) shows an ultrafast 2 ps intermediate (Figure 5b and 6b). Based on previous work on Pt,[13] the observed shift to lower energy and the decreased intensity of the white line peak of the 1 ps transient spectrum qualitatively indicates a reduced state of the metal center when compared to the ground-state spectrum (Figure 6b).[42] Due to the ligand to metal charge transfer (LMCT), charge could be injected from ligands to Pt (Figure 3); thus, reducing the charge difference and hence the chemical bonding likely results in a less intense Pt L_3-edge. Therefore, the transient Pt L_3-edge XANES at 1 ps directly shows the formation of a reduced Pt center from the $Pt^{IV}Cl_6^{2-}$ ground state in water after 266 nm photoexcitation, which is herein ascribed to the generation of Pt(III). Based on our 266 nm (4.66 eV) laser pump, and the extracted lifetime, the fs-TR-XAS suggests a fingerprint for the $[Pt^{III}Cl_5^{2-}(C_{4\,V})\cdots Cl^{\bullet}]$ Adamson's primary radical, or the $Pt^{III}Cl_5^{2-}(C_{4\,V})$ complex proposed by Goursot.[36] Further TR-XAS studies at the Pt L_3-edge pumped with UV and visible light wavelengths in both water and methanol supported by first-principles XAS simulations are required to resolve the precise nature of the intermediates.

CONCLUSION

The polycapillary X-ray spectrometer (PCXS) introduced in this work establishes a new frontier for time-resolved X-ray absorption spectroscopy at XFELs. By combining a large solid-angle polycapillary collection and energy-selective graphite analyzers, the PCXS overcomes one of the primary challenges in XFEL-based fluorescence measurements: the suppression of overwhelming scattering backgrounds in dilute, liquid-phase systems with the efficient collection of X-ray fluorescence photons at low concentrations. This achievement enables measurements that are both selective and sufficiently intense to be acquired within practical beamtime constraints. We demonstrate, for the first time, the ability to perform femtosecond-resolved XAS on sub-millimolar samples at an XFEL, exemplified by the 1 ps Pt L_3-edge dynamics of 0.1 mM hexachloroplatinate in aqueous solution. The ability to resolve such dynamics in minutes of acquisition time opens the door to previously inaccessible classes of samples, including photocatalysts, metalloenzymes, and short-lived intermediates, for which low concentrations have historically made ultrafast spectroscopy infeasible. This capability was realized through the synergistic use of SSRL and LCLS, whose colocation enabled iterative refinement under steady-state conditions and seamless transition to femtosecond-resolved measurements, ensuring both rigor and readiness for XFEL application. With this advancement, XFEL-based X-ray spectroscopy can now be applied to answer real-world questions in chemistry and biochemistry—from catalytic mechanisms to biological redox processes—bringing ultrafast structural and electronic insight into systems whose study had long remained out of reach.

METHODS

Materials. The samples consist of 0.1, 1.0, and 20 mM $[Fe(terpy)_2]^{2+}$ (terpy: 2,2′:6′,2″-terpyridine), and 0.1, 1.0, and 20 mM K_2PtCl_6 aqueous solutions (Milli-Q water, >18 MΩ, <10 ppb TOC). Additionally, 0.1, 1.0, and 20 mM $K_3Fe(CN)_6$, and 0.1, 1.0, and 20 mM K_2PtCl_4 aqueous solutions were prepared to characterize the polycapillary optics properties. All of the chemicals were procured from Sigma-Aldrich and were used without further modifications. The polycapillary optics were acquired from a XOS.

SSRL. XAS experiments at the undulator-based (87-period, 22 mm/period) SSRL beamline 15-2 were performed using a Si(111) crystal monochromator (≈3×10^{13} photons/s, ≈1 eV resolution at 7 keV). A Rh-coated KB mirror pair (3.5 mrad) delivered a monochromatic X-ray beam with size of ≈8×37 μm^2. The calibration of the monochromator was performed with Fe K-edge XAS measured in transmission mode with a photodiode (Hamamatsu S3204-09) and by setting its first inflection point to 7112.0 eV.[19,32] The sample was delivered via a recirculating round 100 μm liquid jet.[19] The sample was prepared as an aqueous solution of 0.1 mM $[Fe(terpy)_2]^{2+}$ complex (2,2′:6′,2″-terpyridine). In the standard measurement mode, the total fluorescence yield (TFY) XAS of the standard reference material was recorded by using the PIPS photodiode (20 mm diameter) typically employed at LCLS. A proof-of-concept was performed by measuring the partial fluorescence yield (PFY) using a single PCO and one highly oriented pyrolytic graphite (HOPG) analyzer crystal with a PILATUS 300k detector. The Fe K-edge XAS was recorded with a single scan with one second acquisition per energy point using the same measurement parameters for both the partial and total fluorescence yield detection modes.

LCLS. Ultrafast XAS at the Pt L_3-edge was measured at the X-ray pump-probe (XPP) and the X-ray correlation spectroscopy (XCS) instruments at the Linac Coherent Light Source

https://doi.org/10.1021/photonsci.5c00024
Photon Sci. 2026, 1, 121−129

(LCLS).[17−19,22] The aqueous hexachloroplatinate samples were delivered in a 100 μm horizontal round liquid jet configuration using an HPLC pump.[19] The liquid jet instrument supplied a fresh sample after each X-ray pulse of the 120 Hz LCLS repetition rate. The incident X-ray beam was monochromatized with a Si(111) crystal monochromator (~30 fs, ~1.4 × 10^{-4} $\Delta E/E$, ~10^{10} photons per pulse) and focused to ~20 μm at the sample's interaction point using a set of Beryllium lenses. In the XCS and XPP standard configurations, the X-ray absorption signal is typically measured in TFY mode with an ePix100 detector. A region of interest (ROI) is defined in the detector to integrate the TFY signal. The intensity of the incident X-ray beam is extracted via the diffuse scattering of the solvent (e.g., water) using epix10K (I0). It enables shot to shot normalization to fluctuations of the incident X-ray intensity and perturbations of the liquid jet.[17,18] Time-resolved Pt L_3-edge was recorded following 266 nm pump laser pulses (Ti:sapphire laser) with an energy of 2 to 27 μJ focused to a 150 μm (XPP) or 120 μm (XCS) full width half maxima at the sample's interaction point, maintaining spatial overlap between the laser and the XFEL beam. An energy dose in the μJ range is typically suitable for liquid-phase photochemistry, and a power titration control experiment was performed to operate within the linear regime without promoting nonlinear events. The time-tool measures a fraction of the beam to determine the time delay between the laser pulse and the XFEL. The laser pump propagates with the X-ray probe with a 2° angle at the sample's position. A detailed description on how to obtain temporal and spatial overlap at the XCS/XPP instruments was reported elsewhere.[17−19,22]

AUTHOR INFORMATION

Corresponding Authors

Dimosthenis Sokaras − *SLAC National Accelerator Laboratory, Menlo Park, California 94025, United States;* orcid.org/0000-0001-8117-1933; Email: dsokaras@slac.stanford.edu

Roberto Alonso-Mori − *SLAC National Accelerator Laboratory, Menlo Park, California 94025, United States;* orcid.org/0000-0002-5357-0934; Email: robertoa@slac.stanford.edu

Authors

Angel T. Garcia-Esparza − *SLAC National Accelerator Laboratory, Menlo Park, California 94025, United States;* orcid.org/0000-0002-4884-171X

Jinkyu Lim − *SLAC National Accelerator Laboratory, Menlo Park, California 94025, United States; Department of Chemical & Biological Engineering, Hanbat National University, Daejeon 34158, South Korea;* orcid.org/0000-0002-1875-659X

Alexander Britz − *SLAC National Accelerator Laboratory, Menlo Park, California 94025, United States;* orcid.org/0000-0002-1049-2841

Marco Reinhard − *SLAC National Accelerator Laboratory, Menlo Park, California 94025, United States;* orcid.org/0000-0001-7155-2011

Ryan D. Ribson − *SLAC National Accelerator Laboratory, Menlo Park, California 94025, United States;* orcid.org/0000-0002-3755-5777

Jeffrey T. Babicz, Jr. − *SLAC National Accelerator Laboratory, Menlo Park, California 94025, United States*

Cali Antolini − *SLAC National Accelerator Laboratory, Menlo Park, California 94025, United States*

Leland B. Gee − *SLAC National Accelerator Laboratory, Menlo Park, California 94025, United States;* orcid.org/0000-0002-5817-3997

Quinn Claussen − *SLAC National Accelerator Laboratory, Menlo Park, California 94025, United States*

Nina A. Boiadjieva − *SLAC National Accelerator Laboratory, Menlo Park, California 94025, United States*

Leslie Hsiao − *SLAC National Accelerator Laboratory, Menlo Park, California 94025, United States*

Jim Defever − *SLAC National Accelerator Laboratory, Menlo Park, California 94025, United States*

Patrick Oppermann − *SLAC National Accelerator Laboratory, Menlo Park, California 94025, United States*

Vincent Esposito − *SLAC National Accelerator Laboratory, Menlo Park, California 94025, United States*

Hasan Yavas − *SLAC National Accelerator Laboratory, Menlo Park, California 94025, United States*

Dean Skoien − *SLAC National Accelerator Laboratory, Menlo Park, California 94025, United States*

Matthieu Chollet − *SLAC National Accelerator Laboratory, Menlo Park, California 94025, United States;* orcid.org/0000-0002-9629-890X

Tim B. van Driel − *SLAC National Accelerator Laboratory, Menlo Park, California 94025, United States;* orcid.org/0000-0003-4070-3168

Sanghoon Song − *SLAC National Accelerator Laboratory, Menlo Park, California 94025, United States*

Diling Zhu − *SLAC National Accelerator Laboratory, Menlo Park, California 94025, United States*

Complete contact information is available at: https://pubs.acs.org/10.1021/photonsci.5c00024

Author Contributions

[▽]A.T.G.-E. and J.L. contributed equally.

Notes

The authors declare no competing financial interest.

ACKNOWLEDGMENTS

Use of the Linac Coherent Light Source, and the Stanford Synchrotron Radiation Lightsource, SLAC National Accelerator Laboratory, was supported by the U.S. Department of Energy, Office of Science, Office of Basic Energy Sciences under Contract no. DE-AC02-76SF00515. This work was supported by NIH grant P41GM139687.

REFERENCES

(1) Guilherme Buzanich, A. Recent developments of X-ray absorption spectroscopy as analytical tool for biological and biomedical applications. *X-Ray Spectrometry* **2022**, *51*, 294−303.

(2) Sokaras, D. A seven-crystal Johann-type hard x-ray spectrometer at the Stanford Synchrotron Radiation Lightsource. *Review of Scientific Instruments* **2013**, *84*, 053102.

(3) Chatterjee, R.; et al. XANES and EXAFS of dilute solutions of transition metals at XFELs. *J. Synchrotron. Radiat.* **2019**, *26*, 1716−1724.

(4) Bergmann, U.; et al. Using X-ray free-electron lasers for spectroscopy of molecular catalysts and metalloenzymes. *Nature Reviews Physics* **2021**, *3* (4), 264−282.

(5) Lin, F.; et al. Synchrotron X-ray Analytical Techniques for Studying Materials Electrochemistry in Rechargeable Batteries. *Chem. Rev.* **2017**, *117*, 13123−13186.

(6) Timoshenko, J.; Roldan Cuenya, B. In Situ/ Operando Electrocatalyst Characterization by X-ray Absorption Spectroscopy. *Chem. Rev.* **2021**, *121*, 882−961.
(7) Emma, P.; et al. First lasing and operation of an ångstrom-wavelength free-electron laser. *Nat. Photonics* **2010**, *4* (9), 641−647.
(8) Kroll, T.; et al. X-ray absorption spectroscopy using a self-seeded soft X-ray free-electron laser. *Opt. Express* **2016**, *24* (20), 22469−22480.
(9) White, W. E.; Robert, A.; Dunne, M. The Linac Coherent Light Source. *urn:issn:1600-5775* **2015**, *22*, 472−476.
(10) Takanabe, K. Photocatalytic Water Splitting: Quantitative Approaches toward Photocatalyst by Design. *ACS Catal.* **2017**, *7*, 8006−8022.
(11) Qureshi, M.; et al. Contribution of electrolyte in nanoscale electrolysis of pure and buffered water by particulate photocatalysis. *Sustain Energy Fuels* **2018**, *2*, 2044−2052.
(12) Chung, T.; et al. Ultrafast X-ray Absorption Spectroscopy Reveals Excited-State Dynamics of B12 Coenzymes Controlled by the Axial Base. *J. Phys. Chem. B* **2024**, *128*, 1428−1437.
(13) Hersbach, T. J. P.; et al. Base-Accelerated Degradation of Nanosized Platinum Electrocatalysts. *ACS Catal.* **2021**, *11*, 9904−9915.
(14) Haumann, M.; et al. Biochemistry: Photosynthetic O2 formation tracked by time-resolved x-ray experiments. *Science (1979)* **2005**, *310*, 1019−1021.
(15) Kern, J.; et al. Structures of the intermediates of Kok's photosynthetic water oxidation clock. *Nature* **2018**, *563* (7731), 421−425.
(16) Cinco, R. M.; et al. Comparison of the manganese cluster in oxygen-evolving photosystem II with distorted cubane manganese compounds through X-ray absorption spectroscopy. *Inorg. Chem.* **1999**, *38*, 5988−5998.
(17) Alonso-Mori, R.; et al. The X-ray Correlation Spectroscopy instrument at the Linac Coherent Light Source. *urn:issn:1600-5775* **2015**, *22*, 508−513.
(18) Chollet, M.; et al. The X-ray Pump−Probe instrument at the Linac Coherent Light Source. *urn:issn:1600-5775* **2015**, *22*, 503−507.
(19) Antolini, C. The Liquid Jet Endstation for Hard X-ray Scattering and Spectroscopy at the Linac Coherent Light Source. *Molecules* **2024**, *29*, 2323.
(20) Britz, A.; et al. Resolving structures of transition metal complex reaction intermediates with femtosecond EXAFS. *Physical Chemistry Chemical Physics* **2020**, *22*, 2660−2666.
(21) Reinhard, M.; et al. Ferricyanide photo-aquation pathway revealed by combined femtosecond Kβ main line and valence-to-core x-ray emission spectroscopy. *Nat. Commun.* **2023**, *14*, 2443.
(22) Alonso-Mori, R.; et al. Photon-in photon-out hard X-ray spectroscopy at the Linac Coherent Light Source. *J. Synchrotron Radiat.* **2015**, *22*, 612−620.
(23) Zimmermann, P.; et al. Modern X-ray spectroscopy: XAS and XES in the laboratory. *Coord Chem. Rev.* **2020**, *423*, 213466.
(24) Bogacz, I.; et al. X-ray Absorption Spectroscopy of Dilute Metalloenzymes at X-ray Free-Electron Lasers in a Shot-by-Shot Mode. *J. Phys. Chem. Lett.* **2025**, *16*, 3778−3787.
(25) Alonso-Mori, R.; et al. A multi-crystal wavelength dispersive x-ray spectrometer. *Review of Scientific Instruments* **2012**, *83*, 073114.
(26) Reinhard, M.; et al. Observation of a Picosecond Light-Induced Spin Transition in Polymeric Nanorods. *ACS Nano* **2024**, *18*, 15468−15476.
(27) Reinhard, M. E.; et al. Time-Resolved X-ray Emission Spectroscopy and Synthetic High-Spin Model Complexes Resolve Ambiguities in Excited-State Assignments of Transition-Metal Chromophores: A Case Study of Fe-Amido Complexes. *J. Am. Chem. Soc.* **2024**, *146*, 17908−17916.
(28) Mara, M. W.; et al. Deciphering Charge Transfer Processes in Transition Metal Complexes from the Perspective of Ultrafast Electronic and Nuclear Motions. *J. Phys. Chem. Lett.* **2024**, *15*, 5250−5258.
(29) Powers-Riggs, N. E.; et al. Characterization of Deformational Isomerization Potential and Interconversion Dynamics with Ultrafast X-ray Solution Scattering. *J. Am. Chem. Soc.* **2024**, *146*, 13962−13973.
(30) Cammarata, M.; et al. Charge transfer driven by ultrafast spin transition in a CoFe Prussian blue analogue. *Nat. Chem.* **2021**, *13*, 10−14.
(31) Van Driel, T. B.; et al. Atomistic characterization of the active-site solvation dynamics of a model photocatalyst. *Nat. Commun.* **2016**, *7*, 13678.
(32) Reinhard, M.; et al. Solution phase high repetition rate laser pump x-ray probe picosecond hard x-ray spectroscopy at the Stanford Synchrotron Radiation Lightsource. *Structural Dynamics* **2023**, *10*, 054304.
(33) Canton, S. E.; et al. Probing the anisotropic distortion of photoexcited spin crossover complexes with picosecond X-ray absorption spectroscopy. *J. Phys. Chem. C* **2014**, *118*, 4536−4545.
(34) Zhang, X.; et al. Dynamic Jahn-Teller effect in the metastable high-spin state of solvated [Fe(terpy)2]2+. *J. Phys. Chem. C* **2015**, *119*, 3312−3321.
(35) Vankó, G.; et al. Detailed characterization of a nanosecond-lived excited state: X-ray and theoretical investigation of the quintet state in photoexcited [Fe(terpy)2]2+. *J. Phys. Chem. C* **2015**, *119*, 5888−5902.
(36) Glebov, E. M.; Pozdnyakov, I. P.; Plyusnin, V. F.; Khmelinskii, I. Primary reactions in the photochemistry of hexahalide complexes of platinum group metals: A minireview. *Journal of Photochemistry and Photobiology C: Photochemistry Reviews* **2015**, *24*, 1−15.
(37) Zheldakov, I. L. *Ultrafast Photophysics and Photochemistry Of Hexacoordinated Bromides of Pt(IV), Os(IV), and, Ir(IV) in the Condensed Phase Studied by Femtosecond Pump-Probe Spectroscopy*. Ph.D. Dissertation, Bowling Green State University, Bowling Green, OH, 2010.
(38) Glebov, E. M.; et al. Redox processes in photochemistry of Pt(iv) hexahaloid complexes. *RSC Adv.* **2012**, *2*, 5768−5778.
(39) Glebov, E. M.; et al. Chain processes in the photochemistry of PtIV halide complexes in aqueous solutions. *Russian Chemical Bulletin* **2013**, *62*, 1540−1548.
(40) Sen, A.; Matthews, E. M.; Hou, G. L.; Wang, X. B.; Dessent, C. E. H. Photoelectron spectroscopy of hexachloroplatinate-nucleobase complexes: Nucleobase excited state decay observed via delayed electron emission. *J. Chem. Phys.* **2015**, *143*, 184307.
(41) Matthews, E.; Sen, A.; Yoshikawa, N.; Bergström, E.; Dessent, C. E. H. UV laser photoactivation of hexachloroplatinate bound to individual nucleobases: In vacuo as molecular level probes of a model photopharmaceutical. *Physical Chemistry Chemical Physics* **2016**, *18*, 15143−15152.
(42) Hersbach, T. J. P.; et al. Platinum hydride formation during cathodic corrosion in aqueous solutions. *Nat. Mater.* **2025**, *24*, 574−580.

https://doi.org/10.1021/photonsci.5c00024
Photon Sci. 2026, 1, 121−129